electronic reprint

Journal of
**Applied
Crystallography**
ISSN 0021-8898

Tracking: a method for structural characterization of grains in powders or polycrystals

E. M. Lauridsen, S. Schmidt, R. M. Suter and H. F. Poulsen

Copyright © International Union of Crystallography

Author(s) of this paper may load this reprint on their own web site provided that this cover page is retained. Republication of this article or its storage in electronic databases or the like is not permitted without prior permission in writing from the IUCr.

Journal of
Applied
Crystallography
ISSN 0021-8898

Received 28 March 2001
Accepted 29 August 2001

Tracking: a method for structural characterization of grains in powders or polycrystals

E. M. Lauridsen,[a] S. Schmidt,[a] R. M. Suter[b] and H. F. Poulsen[a]*

[a]Materials Research Department, Risø National Laboratory, DK-4000 Roskilde, Denmark, and [b]Department of Physics, Carnegie Mellon University, Pittsburgh, PA 15213, USA. Correspondence e-mail: henning.friis.poulsen@risoe.dk

© 2001 International Union of Crystallography
Printed in Great Britain – all rights reserved

A method is presented for fast and non-destructive characterization of the individual grains inside bulk materials (powders or polycrystals). The positions, volumes and orientations of hundreds of grains are determined simultaneously. An extension of the rotation method is employed: a monochromatic beam of high-energy X-rays, focused in one dimension, impinges on the sample and the directions of the diffracted beams are traced by translation of two-dimensional detectors. Algorithms suitable for on-line analysis are described, including a novel indexing approach, where the crystal symmetry is used directly by scanning in Euler space. The method is verified with a simulation of 100 grains.

1. Introduction

Many of the properties of metals and ceramics are determined by the structure and interactions of individual grains. Both in powders and polycrystalline materials, the agglomerate is often highly heterogeneous with grains varying in size, shape, crystallographic orientation and stress state, as well as in their relationships to neighbouring grains. As such, it is remarkable that state-of-the-art models in general only deal with average properties. A major cause for this situation is the almost exclusive use of surface probes (electron microscopy and standard laboratory X-ray diffraction) for structural characterization. Due to surface effects such as strain relaxation, pinning and atypical diffusion, samples must be treated and then sectioned before investigation to obtain results representative of bulk behaviour. This destructive procedure prohibits studies of the dynamics of individual grains. Hence, only static and statistical information is obtained.

A need is therefore identified for a non-destructive technique that provides three-dimensional mappings of the pertinent grain characteristics. The technique must enable analysis over an ensemble of 10–1000 grains for significant conclusions to be drawn. Likewise, the data acquisition speed must be sufficient to perform *in situ* processing studies.

We present here an X-ray diffraction technique that fulfils the above requirements. By coupling the monochromatic 'rotation method' with ray tracing, the positions, volumes and orientations of hundreds of grains are determined simultaneously. The technique is limited to undeformed or weakly deformed samples with grains exhibiting a mosaic spread of less than a few degrees. Kinematical diffraction is assumed. The technique applies to all X-ray energies, but emphasis is on the use of high energies, $E > 40$ KeV. These provide the necessary penetration power for three-dimensional mapping of bulk hard condensed matter (Bouchard *et al.*, 1998; Poulsen *et al.*, 1997), and extinction is in general negligible. The technique is named 'tracking' by analogy to reconstruction procedures in particle physics.

First results based on parts of this methodology and a few grains have been presented elsewhere (Lauridsen *et al.*, 2000; Juul Jensen *et al.*, 2000; Juul Jensen & Poulsen 2000; Nielsen, Ludwig *et al.*, 2000; Margulies, Winther *et al.*, 2001; Margulies, Lorentzen *et al.*, 2001). This article gives a comprehensive view of the tracking technique, emphasizing the situation with many grains. As the main topic, an algorithm is developed for sorting and analyzing the vast quantity of data produced. The outcome is a program called *GRAINDEX*, which has been implemented at the three-dimensional X-ray diffraction (3DXRD) microscope at beamline ID11, European Synchrotron Radiation Facility (ESRF) (Lienert *et al.*, 1999). The algorithm is outlined in Fig. 1. Initially, all grains are associated with the same *a priori* known space group and lattice parameters, representing, for example, a stoichiometric and strain-free reference material. The ray tracing provides a list of reflections characterized by their centre-of-mass origin and integrated intensity. The reflections are sorted with respect to their grain of origin by the central indexing algorithm. Next, the positions, volumes and crystallographic orientations of the grains can be fitted.

Once the grains are indexed, single-crystal refinements may be applied. Alternatively, the relevant part of the data may be reinvestigated for a stress analysis. Depending on grain size, it may also be possible to produce a three-dimensional map of grain boundaries. These topics will be treated in a following publication. First examples of grain-boundary mapping and strain data have been reported by Nielsen, Ludwig *et al.* (2000) and Margulies, Lorentzen *et al.* (2001), respectively.

The article will follow the flow of the data analysis. Having established the geometry, we present details of the tasks identified in Fig. 1. Emphasis is on a fast indexing routine,

electronic reprint

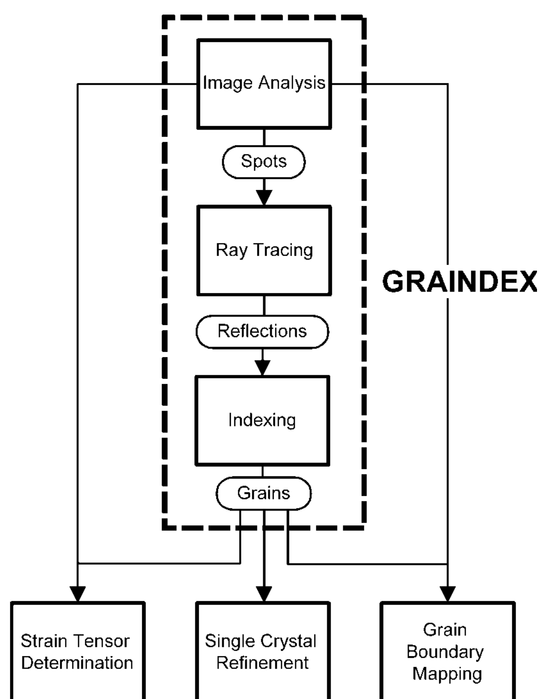

Figure 1
A flow chart for the tracking method using the *GRAINDEX* algorithm. *GRAINDEX* generates a list of grains with associated positions and orientations as well as sets of indexed reflections with associated integrated intensities. The output may be used for crystallographic refinements of the grains or, with a reanalysis of the raw data, for determining the average strain tensors. Furthermore, for coarse-grained materials the grain boundaries can be mapped in three dimensions.

enabling on-line data analysis. Finally, limitations are discussed based on results of a computer simulation.

2. Tracking principle

The experimental geometry is sketched in Fig. 2. The sample is mounted on an ω rotation stage. A beam of monochromatic high-energy X-rays is focused in one direction in order to define a layer in the sample, which is perpendicular to the ω rotation axis. Some of the grains intersected by this layer will give rise to diffracted beams, which are transmitted through the sample to be observed as spots by a flat two-dimensional detector. The detector is aligned perpendicular to the incident beam. In addition, an optional slit is placed before the sample.

The tracking algorithm works as follows. Images are acquired at a number of rotation-axis-to-detector distances, L_1 to L_N (typically $N = 3$). Equivalent spots, generated by the same reflection, are identified and a best fit is determined to a line through the centre-of-mass (CM) positions of these spots. This determines the scattered wavevector, which we specify in terms of the scattering angle, 2θ, and the azimuthal angle, η. Extrapolating the fitted line to its intersection with the incident beam determines the CM position of the illuminated section of the grain of origin, specified by (x_l, y_l). For definitions of zero points and positive directions, see Fig. 2.

To obtain information from all grains in one layer, the X-ray tracing is repeated at a number of ω settings in steps of $\Delta\omega$. During each exposure, the sample is oscillated by $\pm\Delta\omega/2$. Typically, an ω range of 25–40° provides a sufficient number of Bragg peaks from each grain. If the ω range is expanded to 180°, all reflections are illuminated with the exception of those lying in two small 'blind' spots on the unit sphere (centred on the ω axis) with a total spherical area of $4\pi[1 - \cos(\theta)]$, where θ is the Bragg angle. For high-energy X-rays with wavelength, λ, much less than the lattice constant, this area is negligible for low-order reflections. This observation justifies the use of a sample stage with only one rotation.

Finally, for a complete mapping, the procedure is repeated for a set of layers by translating the sample in z. In this way a six-dimensional space, consisting of the $(x, y, z, \omega, 2\theta, \eta)$ coordinates for the various reflections, is probed with essentially a two-dimensional scan over ω and z.

As a variation of the tracking method, we consider the monochromatic beam being restricted in two directions, either by focusing or by slits. This is an option if the overlap between spots arising from the grains in the full layer is too severe. For each ω setting, the beam then defines a stripe through the sample. Upon rotation, only grains close to the rotation axis will remain fully illuminated. The majority of the spots therefore need to be discarded from the analysis, and a full mapping requires additional scanning with translations x and y on top of the rotation table.

In the following, as default we will assume that the beam defines an ideal horizontal plane. Furthermore, we assume that the energy bandwidth and divergence of the beam are negligible. (As an example, the numbers for the 3DXRD instrument are at most 0.1% and 0.5 mrad, which leads to negligible contributions to the uncertainty in Euler angle determination.)

3. Coordinate transformations

The algebra for associating scattering observations with reciprocal space is well described for single crystals (Busing & Levy, 1967). The polycrystal case differs by the need for one extra coordinate system since the sample and grains are different objects. For reference purposes we present the equations, following the single-crystal formalism of Busing & Levy (1967) as close as possible (our sign convention for ω, however, is opposite to theirs). Four Cartesian coordinate systems are introduced: the laboratory system, the ω-axis system, the sample system and the Cartesian grain system.

We describe the coordinate transformations for an arbitrary scattering vector, $\mathbf{G}$. The laboratory system $(\mathbf{x}_l, \mathbf{y}_l, \mathbf{z}_l)$ is defined in Fig. 2. It has $\mathbf{x}_l$ pointing along the incoming beam, $\mathbf{y}_l$ transverse to it in the horizontal plane and $\mathbf{z}_l$ positive upwards, parallel to the ω rotation axis. In this system, vectors are given the subscript l: $\mathbf{G}_l$. The ω system $(\mathbf{x}_\omega, \mathbf{y}_\omega, \mathbf{z}_\omega)$ is rigidly attached to the ω turntable. For $\omega = 0$, the ω and laboratory systems are the same. Hence, the scattering vector transforms as $\mathbf{G}_l = \mathbf{\Omega}\mathbf{G}_\omega$ with

electronic reprint

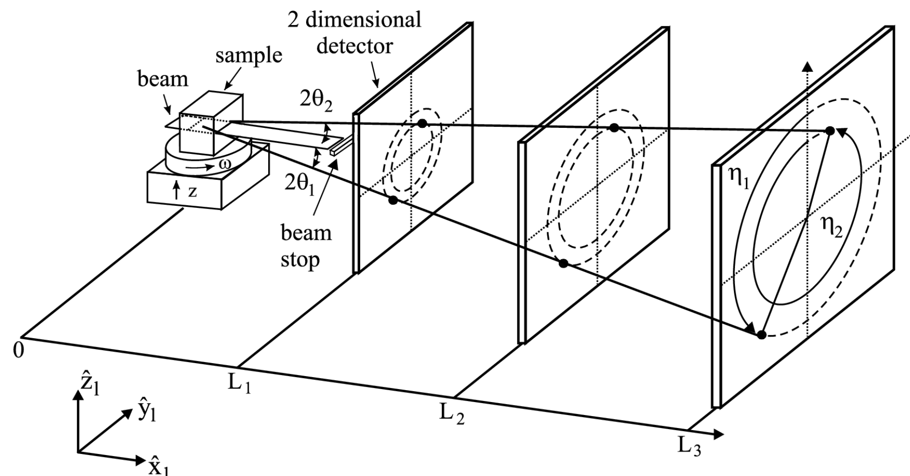

Figure 2
Illustration of the tracking principle. Spots arising from the same reflection at different sample–detector distances are identified. Linear fits through these are extrapolated to give the position of the grain within the illuminated layer in the sample. The angles (2θ, η, ω) are defined, as well as the laboratory coordinate system ($\mathbf{x}_l$, $\mathbf{y}_l$, $\mathbf{z}_l$).

$$\boldsymbol{\Omega} = \begin{bmatrix} \cos(\omega) & -\sin(\omega) & 0 \\ \sin(\omega) & \cos(\omega) & 0 \\ 0 & 0 & 1 \end{bmatrix}. \qquad (1)$$

The sample system ($\mathbf{x}_s$, $\mathbf{y}_s$, $\mathbf{z}_s$) is fixed with respect to the sample, *e.g.* defined by deformation axes (RD, TD, ND). The orientation of the sample on the ω turntable is given by the **S** matrix: $\mathbf{G}_\omega = \mathbf{S}\mathbf{G}_s$. **S** must be provided by the user and is typically used to swap axes, in order to simplify the data analysis.

The crystallographic orientation of a grain with respect to the sample is given by the **U** matrix: $\mathbf{G}_s = \mathbf{U}\mathbf{G}_c$, where index c refers to the Cartesian grain system ($\mathbf{x}_c$, $\mathbf{y}_c$, $\mathbf{z}_c$). This is fixed with respect to the reciprocal lattice ($\mathbf{a}^*$, $\mathbf{b}^*$, $\mathbf{c}^*$) in the grain. We use the convention that $\mathbf{x}_c$ is parallel to $\mathbf{a}^*$, $\mathbf{y}_c$ is in the plane of $\mathbf{a}^*$ and $\mathbf{b}^*$, and $\mathbf{z}_c$ is perpendicular to that plane. Let **G** be represented in the reciprocal-lattice system by the Miller indices $\mathbf{G}_{hkl} = (h, k, l)$. The correspondence between the Cartesian grain system and reciprocal space is then given by the **B** matrix: $\mathbf{G}_c = \mathbf{B}\mathbf{G}_{hkl}$, with

$$\mathbf{B} = \begin{bmatrix} a^* & b^*\cos(\gamma^*) & c^*\cos(\beta^*) \\ 0 & b^*\sin(\gamma^*) & -c^*\sin(\beta^*)\cos(\alpha) \\ 0 & 0 & c^*\sin(\beta^*)\sin(\alpha) \end{bmatrix} \qquad (2)$$

and

$$\cos(\alpha) = \frac{\cos(\beta^*)\cos(\gamma^*) - \cos(\alpha^*)}{\sin(\alpha^*)\sin(\beta^*)}. \qquad (3)$$

Here ($a, b, c, \alpha, \beta, \gamma$) and ($a^*, b^*, c^*, \alpha^*, \beta^*, \gamma^*$) symbolize the lattice parameters in direct and reciprocal space, respectively.

The orientation matrix **U** can be parameterized in numerous ways (well known from texture analysis). As default, we use the (ϕ, φ_1, φ_2) Euler angle notation (Bunge, 1982):

$$\begin{pmatrix} \mathbf{U}_{11} & \mathbf{U}_{12} & \mathbf{U}_{13} \\ \mathbf{U}_{21} & \mathbf{U}_{22} & \mathbf{U}_{23} \\ \mathbf{U}_{31} & \mathbf{U}_{32} & \mathbf{U}_{33} \end{pmatrix} = \begin{bmatrix} \cos(\varphi_1)\cos(\varphi_2) - \sin(\varphi_1)\sin(\varphi_2)\cos(\phi) & -\cos(\varphi_1)\sin(\varphi_2) - \sin(\varphi_1)\cos(\varphi_2)\cos(\phi) & \sin(\varphi_1)\sin(\phi) \\ \sin(\varphi_1)\cos(\varphi_2) + \cos(\varphi_1)\sin(\varphi_2)\cos(\phi) & -\sin(\varphi_1)\sin(\varphi_2) + \cos(\varphi_1)\cos(\varphi_2)\cos(\phi) & -\cos(\varphi_1)\sin(\phi) \\ \sin(\varphi_2)\sin(\phi) & \cos(\varphi_2)\sin(\phi) & \cos(\phi) \end{bmatrix} \qquad (4)$$

Equations and diagrams with reference to pole figures and the high-energy X-ray setup can be found in work by Mishin *et al.* (2000).

Next, we deduce the basic diffractometer equations. In order for a given scattering vector **G** to give rise to a diffraction spot it must fulfil Bragg's law:

$$|\mathbf{G}| = 4\pi\sin(\theta)/\lambda. \qquad (5)$$

From the geometry in Fig. 2 we have

$$\mathbf{G}_l = \frac{2\pi}{\lambda}\begin{bmatrix} \cos(2\theta) - 1 \\ -\sin(2\theta)\sin(\eta) \\ \sin(2\theta)\cos(\eta) \end{bmatrix}. \qquad (6)$$

The coordinate transforms introduced above lead to

$$\mathbf{G}_l = \boldsymbol{\Omega}\mathbf{SUBG}_{hkl}. \qquad (7)$$

4. Image analysis and X-ray tracing

Initially all images are scanned for bright objects that satisfy certain criteria on area, connectivity and maximum intensity. These criteria depend on the experimental conditions and generally have to be found by trial-and-error. Additional criteria may apply, such as the location of an object in the image. Objects meeting the criteria are defined as spots. Spots

electronic reprint

are associated with a CM pixel position, an ω position (the middle of the $\Delta\omega$ interval) and an integrated intensity.

Depending on mosaic spread, the same reflections may give rise to spots appearing at several consecutive ω settings. *GRAINDEX* identifies such groups as single spots, adds integrated intensities and assigns pixel positions and ω positions based on weighted averages.

Next, valid spots in images acquired at different detector distances are grouped into a reflection and the linear fitting (orthogonal regression) is performed. Three criteria are applied to discriminate against erroneous groupings, typically caused by spot overlap. First, tolerances are set on the χ^2 of the fit and the variation in integrated intensity within corresponding spots. Second, the fitted 2θ value is compared with calculated ones. If the observed value matches, within a tolerance, one of the calculated values, the reflection is put in a list with others of that $\{hkl\}$ family; otherwise it is disregarded. If the observed 2θ could be associated with more than one $\{hkl\}$, list entries corresponding to each $\{hkl\}$ family are created. The erroneous reflections are sorted out later. Third, the fitted CM origin obtained by extrapolation of the fitted line to the incident beam plane should be positioned within the illuminated region of the sample.

The integrated intensity of the reflection is taken to be that of the outermost L setting. For comparison between reflections it is multiplied by polarization Debye–Waller and Lorentz factors. With our conventions the Lorentz factor is

$$\mathrm{Lor}(2\theta, \eta) = 1/[\sin(2\theta)|\sin(\eta)|]. \tag{8}$$

Note that spots appearing near $\eta = 0$ and $\eta = 180^\circ$ have to be discarded as the Lorentz factor is diverging at this point and parts of the mosaic spread may be situated in the inaccessible areas on the unit sphere near the rotation axis. Also such spots will tend to appear at several consecutive ω settings, adding to noise in the summed intensity. In practice, this restriction is handled by defining certain η ranges to be void.

5. Indexing

Indexing is not straightforward, partly because of the overlap of spots, and partly because of their magnitudes. Three criteria may be applied to sort reflections according to grain: the position (x_ω, y_ω), the crystallography, and the integral intensities (area of grain section). Among these, the latter is considered the least robust. One reason is the issue of the 'grains at the boundary'. In many cases, samples will have a plate- or rod-like geometry with dimensions that are too large for the entire section to be illuminated by the incident beam. Hence, there will be a number of grains which will be partly illuminated and which will tend to rotate in and out of the illuminated area. The spots arising from these pieces of grains will still be assigned correct orientations and X-ray tracing will place the CM of the pieces within the area of the full grains. In contrast, the intensities will be reduced. In the limit of the grain dimensions being much larger than the accuracy with which the X-ray tracing defines the CM positions, it is possible to rely primarily on the position criterion.

In the limit of the grains being much smaller than the error on the CM position, indexing must rely on the crystallographic criteria. Let us therefore consider the case of equal-sized grains, all placed at the origin. At first, it seems relevant to compute the angles between all pairs of observed reflections and compare these to a list of allowed angles, dictated by the space-group symmetry. Grains are then defined by groups of reflections, where all pairs mutually fulfil the angle criterion. However, as n reflections give rise to 2^n possible groups, the speed of analysis becomes prohibitive for large n. Instead, space-group symmetry can be probed directly, leading to an algorithm for which the speed is almost independent of n. By rearranging (7) as

$$\mathbf{G}_s = \mathbf{U}\mathbf{B}\mathbf{G}_{hkl}, \tag{9}$$

the measurements of $\mathbf{G}_s$ and crystallographic properties ($\mathbf{B}$, $\mathbf{G}_{hkl}$) are separated. Note that the number, n, of measured reflections $(\mathbf{G}_s)_i$ increases with the number of grains, whereas the number M_0 of theoretical reflections $(\mathbf{B}\mathbf{G}_{hkl})_j$ is constant.

The underlying principle of the algorithm is to scan through all orientations and for each orientation $\mathbf{U}$ count the number, $M_{\rm exp}$, of (hkl)'s for which there is at least one observation $\mathbf{G}_s$ that matches $\mathbf{U}\mathbf{B}\mathbf{G}_{hkl}$. Grains are defined by completeness and uniqueness criteria. The former requires $M_{\rm exp} \geq (1-\alpha)M_0$, where the tolerance α is rather small. The latter requires that the set of matching (hkl)'s is not a sub-set of the set of matching (hkl)'s for another $\mathbf{U}$ setting. Naturally, scanning through all orientations in a strict mathematical sense is not possible. However, by incrementing the three Euler angles defining $\mathbf{U}$ by finite steps *and* allowing a corresponding mismatch between the left- and right-hand sides of (9), the number of orientations to test becomes finite.

To sample Euler space homogeneously, we use the metric (Hansen *et al.*, 1978)

$$\mathrm{d}\mathbf{U}(\phi, \varphi_1, \varphi_2) = (1/8\pi^2)\sin(\phi)\,\mathrm{d}\phi\,\mathrm{d}\varphi_1\,\mathrm{d}\varphi_2. \tag{10}$$

Furthermore, the crystal symmetry of each grain implies that only a subset of the full $[0, \pi] \times [0, 2\pi] \times [0, 2\pi]$ Euler space needs to be sampled. As an example, 1/24 of the volume is sufficient for cubic symmetry and this yields a corresponding increase in speed of the algorithm. For a discussion of the symmetries in Euler space, see work by *e.g.* Randle & Engler (2000).

To allow an effective search for the $(\mathbf{G}_s)_i$'s, initially these are placed in look-up tables, one for each $\{hkl\}$ family. In these, the unit vectors $\mathbf{G}_s/|\mathbf{G}_s|$ are represented by spherical coordinates (ψ_1, ψ_2). For a given $\mathbf{U}\mathbf{B}\mathbf{G}_{hkl}$, an area around the theoretical $(\psi_1, \psi_2)^0$ is searched and the matching observations found (if any). The size of the search area reflects the measuring errors and the step size in the scan over Euler space.

For a given step in Euler space, the calculated $\mathbf{G}_{hkl}$'s are grouped as follows.

Group A: reflections that have no matching observations.

Group B: reflections that have one matching observation.

Group C: reflections that have two or more matching observations.

electronic reprint

Provided that the number of A-type reflections is small enough to fulfil the completeness criteria, a linear least-squares fit is made to the orientation of the grain based on the $\mathbf{G}_s$ vectors associated with group B. To linearize equation (9) in ϕ, φ_1 and φ_2, we expand to first order around the nominal step position in Euler space. Hence, for a given step $(\phi^0, \varphi_1^0, \varphi_2^0)$ and corresponding $\mathbf{U}^0 = \mathbf{U}(\phi^0, \varphi_1^0, \varphi_2^0)$ we have

$$\mathbf{U}_{mn} = \mathbf{U}^0_{mn} + \frac{\delta \mathbf{U}}{\delta \phi}(\mathbf{U}^0)_{mn}\Delta\phi + \frac{\delta \mathbf{U}}{\delta \varphi_1}(\mathbf{U}^0)_{mn}\Delta\varphi_1 + \frac{\delta \mathbf{U}}{\delta \varphi_2}(\mathbf{U}^0)_{mn}\Delta\varphi_2. \qquad (11)$$

For step sizes of a few degrees in ϕ, φ_1 and φ_2, this is an excellent approximation. The fit is weighted with respect to the estimated experimental errors in ω and η:

$$\chi^2 = \sum_{i,j} \frac{\{(\mathbf{G}_s)_j - [\mathbf{U}(\Delta\phi, \Delta\varphi_1, \Delta\varphi_2)\mathbf{B}(\mathbf{G}_{hkl})]_j\}_i^2}{\sigma_{ij}^2(\Delta\omega, \Delta\eta)}. \qquad (12)$$

Here index i runs over the spatial coordinates, $i = 1, 2, 3$, while j enumerates the members of group B. σ_{ij}^2 is the error on $\mathbf{G}_s$ vector number j in the point $\mathbf{U}^0$, calculated by error propagation using equations (1) and (6).

This approach, trusting the group B reflections, has one pitfall. Assume a reflection from the grain to be found is lacking, *e.g.* because of overlap, but one stray reflection is positioned within the same search area in (ψ_1, ψ_2). Then the stray reflection will be assigned as a group B reflection. This reflection is likely to move the least-squares fit minimum substantially as it contributes with a large weight. To discard such 'outliers', the fit is performed in iterative steps using a reweighting scheme. Alternative methods for producing a more robust fit with less or no weight on outliers can be found in the book by Press *et al.* (1992).

The final result of the fit to the group B reflections is used to choose among observations in group C. For a given (hkl), the $\mathbf{G}_s$ observation that is closest and within $\Delta\omega$ and $n\Delta\eta$ of the expected position is chosen (if any).

Returning to the general case of grains of various sizes, which on average are comparable with the error in the CM positions, *GRAINDEX* uses a modification of the Euler scan procedure just outlined. Once an orientation is found fulfilling the completeness criterion, the associated B- and C-type reflections are sorted by CM position and/or integrated intensity.

6. Grain position, volume and orientation

Having indexed the grains, optimized positions and volumes can be found from the set of associated reflections. *GRAINDEX* determines the position as a weighted average of the (x_ω, y_ω) coordinates. The volume is defined by conventional single-crystal refinement. The necessary intensity normalization can be obtained *e.g.* by summing all the reflections from all the grains in the layer of interest, *i.e.* by acquiring data through a complete ω sweep from -90 to $90°$.

The precise determination of the orientation matrix is complicated by the large relative uncertainties on ω. In fact, by simply associating a reflection with the middle position in the $\Delta\omega$ interval, the assumption of Gaussian distributed data underlying least-squares routines fails. Hence, maximum-likelihood methods may be relevant. In practice, *GRAINDEX* does use the least-squares formalism of equation (12), associating errors of $\Delta\omega$ with the ω observations.

7. Simulations

To verify the indexing procedure we have performed Monte Carlo simulations. The grains were assumed to have random orientations and to appear as ideal intensity spikes in the images. Furthermore, they were assumed to be of the same size and to be positioned on top of each other, such that the indexing relied on the crystallographic criteria only. An example of the results is shown in Fig. 3 for 100 grains of f.c.c. symmetry. The simulated data covered an ω range from -45 to $45°$ in steps of $1°$ and included only the four $\{hkl\}$ families with highest d spacings. In total, 2498 reflections were generated. *GRAINDEX* was operated with a $1°$ step in the Euler angles and estimated errors of $\Delta\omega = 0.5°$ and $\Delta\eta = 0.3°$. The completeness and uniqueness criteria were 0.9 and 0.2, respectively. Computing time was 1 min.

Exactly 100 grains were identified and indexed by *GRAINDEX*. Histograms are shown in Fig. 3. These provide statistics over the grain distributions of the completeness factor (the number of reflections found by *GRAINDEX*, correct or not, divided by the number of reflections generated) and purity factor (the number of correct reflections divided by the number of reflections found). The average values for the two distributions are 99.4 and 99.8%, respectively. The result is found to be robust with respect to changes in the *GRAINDEX* parameters.

8. Discussion

The method outlined is implemented at the 3DXRD microscope at beamline ID11, ESRF. This instrument operates in the 50–100 keV range with broadband optics (Lienert *et al.*, 1999). Typically, the line focus is produced with a bent Laue monochromator. With a focal distance of 2 m and a divergence of <0.5 mrad, the spot size is presently 1–2 µm. The flux is sufficient to observe grains of size 0.3 µm (Jensen & Poulsen, 2000). The spatial resolution is mainly limited by the two-dimensional detectors available, which at present have point-spread functions of 20 µm. With typical exposures times of 1 s, one plane in the sample is characterized within a few minutes.

The program *GRAINDEX* runs on a Windows platform. It utilizes the commercial software *Image Pro Plus* for visualization and some of the image analysis tasks. It supports all space groups. Running on a 1.4 GHz Pentium, one layer is indexed within approximately 1 min. Hence, the speed is sufficient for on-line analysis of the positions, volumes and orientations.

electronic reprint

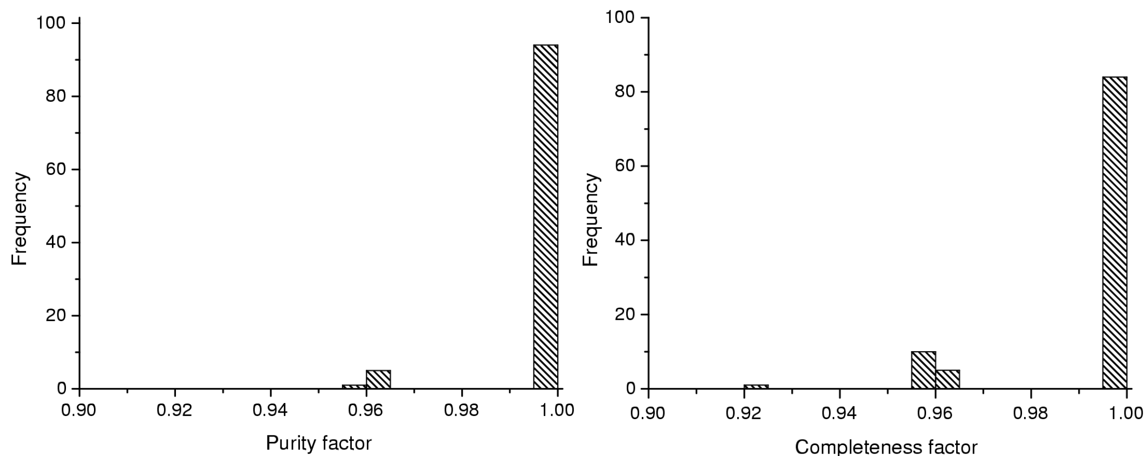

Figure 3
Histograms of the outcome of *GRAINDEX* when provided with input from a simulation of 100 randomly oriented grains (2498 diffraction spots). *GRAINDEX* identified all 100 grains. For each grain, the completeness factor is defined as the number of reflections found (correct or not) divided by the number of reflections generated. Likewise, the purity factor is defined as the number of correct reflections divided by the number of reflections found.

There are three main limitations of the tracking technique. Firstly, deformation will lead to broadening of spots and eventually to spot overlap. The image analysis part then breaks down. So far grains have been partially indexed up to 11% deformation (Margulies *et al.*, 2001). Secondly, even for non-deformed grains there is a limit to the number of spots that can be indexed. In the case of small grains with random orientations in a crystal with cubic symmetry, we estimate that this limit is around 1000. Thirdly, the grains at the boundary of the illuminated volume will give rise to a background of spots, which do not fulfil the completeness criteria. To include these, a more extensive analysis is needed.

One remedy to some of these problems could be to combine tracking with the use of a conical slit (Nielsen, Wolf *et al.*, 2000). The conical slit then defines an interior gauge volume, centred at the ω rotation axis. Only spots arising from this 'area of interest' will reach the detector. Another is to install a slit in front of the sample and monitor the intensity of all the spots as a function of the width of the beam (Lauridsen *et al.*, 2000). Spots arising from grains fully illuminated by the beam are easily identified in this way.

In parallel with the efforts presented here, Ice and coworkers from Oak Ridge National Laboratory have developed a white-beam technique (Chung & Ice, 1999) for studying local texture and strain. Their technique has the intriguing aspect that sample rotation is not needed. However, the number of spots per image increases substantially, leading to a reduced upper limit on the number of grains in the gauge volume. With their point-focus beam, the sample has to be mapped by scanning in both y and z at the expense of speed. With respect to the actual implementation, another major difference is that the Oak Ridge instrument operates with ~20 keV X-rays and shorter focal lengths, enabling better spatial resolution at the expense of a substantially lower penetration power (*e.g.* for Fe the penetration depth is 50 μm and 2100 μm for 20 and 80 keV, respectively) and less space for sample surroundings.

We thank P. Kirkegård, B. S. Johansen, D. Hennessy and C. Xiao for discussions, S. F. Nielsen for manual tests of some of the algorithms, Å. Kvick and G. Vaughan at ESRF for general support, as well as our colleagues U. Lienert, L. Margulies, T. Lorentzen and D. Juul Jensen who took part in experiments. This work was supported by the Danish Natural Science Research Council *via* Dansync. RMS also received support from the MRSEC program of the US National Science Foundation under Award DMR-0079996.

References

Bouchard, R., Hupfeld, D., Lippmann, T., Neuefeind, J., Neumann, H.-B., Poulsen, H. F., Rütt, U., Schmidt, T., Schneider, J. R., Sussenbach, J. & von Zimmermann, M. (1998). *J. Synchrotron Rad.* **5**, 90–101.

Bunge, H. J. (1982). *Texture Analysis in Materials Science.* London: Butterworths.

Busing, W. R. & Levy, H. A. (1967). *Acta Cryst.* **22**, 457–464.

Chung, J.-S. & Ice, G. E. (1999). *J. Appl. Phys.* **86**, 5249–5255.

Hansen, L., Pospiech, J. & Lücke, K. (1978). *Tables of Texture Analysis of Cubic Crystals.* Berlin: Springer-Verlag.

Juul Jensen, D., Kvick, Å., Lauridsen, E. M., Lienert, U., Margulies, L., Nielsen, S. F. & Poulsen, H. F. (2000). *Mater. Res. Soc. Symp. Proc.* **590**, 227–240.

Juul Jensen, D. & Poulsen, H. F. (2000). *Proceedings of the 21st Risø International Symposium on Materials Science*, Roskilde, Denmark, pp. 103–124.

Lauridsen, E. M., Juul Jensen, D., Poulsen, H. F. & Lienert U. (2000). *Scr. Mater.* **43**, 561–566.

Lienert, U., Poulsen, H. F. & Kvick, Å. (1999). *Proceedings of the 40th Conference of AIAA on Structures, Structural Dynamics and Materials*, St Louis, USA, pp. 2067–2075.

Margulies, L., Lorentzen, T., Poulsen, H. F. & Leffers, T. (2001). *Acta Mater.* Submitted.

Margulies, L., Winther, G. & Poulsen, H. F. (2001). *Science*, **291**, 2392–2394.

electronic reprint

Mishin, O. V., Lauridsen, E. M., Krieger Lassen, N. C., Brückner, G., Tschentscher, T., Bay, B., Juul Jensen, D. & Poulsen, H. F. (2000). *J. Appl. Cryst.* **33**, 364–371.
Nielsen, S. F., Ludwig, W., Bellet, D., Lauridsen, E. M., Poulsen, H. F. & Juul Jensen, D. (2000). *Proceedings of the 21st Risø International Symposium on Materials Science*, Roskilde, Denmark, pp. 473–478.
Nielsen, S. F., Wolf, A., Poulsen, H. F., Ohler, M., Lienert, U. & Owen, R. A. (2000). *J. Synchrotron Rad.* **7**, 103–109.
Poulsen, H. F., Garbe, S., Lorentzen, T., Juul Jensen, D., Poulsen, F. W., Andersen, N. H., Frello, T., Feidenhans'l, R. & Graafsma, H. (1997). *J. Synchrotron Rad.* **4**, 147–154.
Press, W. H., Teukolsky, S. A., Vetterling, W. T. & Flannery, B. P. (1992). *Numerical Recipes in FORTRAN*, pp. 694–700. Cambridge University Press.
Randle, V. & Engler, O. (2000). *Introduction to Texture Analysis, Macrotexture, Microtexture and Orientation Mapping.* London: Gordon and Breach.

electronic reprint